Nanoporous Scaffold with Immobilized Enzymes during Flow-Induced Gelation for Sensitive H_2O_2 Biosensing

By *Donglai Lu, Joshua Cardiel, Guozhong Cao,* and *Amy Q. Shen**

Biosensors play indispensible roles in disease diagnosis, drug screening, and forensic applications, while nanoporous scaffolds hold an enormous potential in improving the performance of biosensors.[1] One important area of biosensor research is the immobilization of enzymes with retained or enhanced activities and lifetimes as it is critical to enhance biosensor performance.[2–10] In spite of significant advances made recently for enzyme immobilization such as covalent binding,[3–5] direct adsorption,[6,7] and entrapment in different substrate materials,[8–10] the design of a simple, in-situ, and cost-effective process that can be reliably deployed in immobilization of enzymes while retaining the enzyme's native stabilities and reactivities remains a significant challenge.[11,12] For example, the standard fabrication process for enzyme immobilization is usually very complicated and costly;[3,4,7,10] the immobilized enzyme molecules tend to have non-uniform distribution in the host matrix, easily denature, leach, and lose activities over time. Further, the host matrices are often not highly biocompatible and bristle in nature. Here, we present a novel and versatile flow-induced gelation method to immobilize enzymes inside nanoporous scaffolds to meet these challenges. The biosensor designed by the nanoporous scaffold shows high sensitivity, stability, selectivity, and good precision.

The novel enzyme immobilization method introduced here is based on our recent work of forming stable nanoporous scaffolds with proper hydrodynamic conditions for a given self-assembly precursor (see **Figure 1** and the Supporting Information, SI).[13] When subject to flow, flow-induced structure formation of self-assembled surfactant micelles occurs in a narrow range of concentrations of specific ionic surfactant solutions with added salts. Existing work on phase transitions in macroscopic geometry, has been reported to be reversible under shear flow conditions.[14] However, the major challenge of utilizing shear-induced structures as nanotemplates is the structure breakdown and disintegration once the flow is stopped. We are able to obtain irreversible nanoporous scaffolds by using specially designed microfluidic devices (see Figure 1). The irreversible gel formation results from the large shear and extension strain rates and total strain generated by the flow through the device, under mixed extensional and shear flow conditions. Based on the rheological and hydrodynamics calculations, we identified the irreversible gelation conditions to be $\dot{\gamma} > \dot{\gamma}_c$, $\gamma > \gamma_c$ and $\dot{\varepsilon} > \dot{\varepsilon}_c$, with $\dot{\gamma}$ being the shear rate, γ the strain, and $\dot{\varepsilon}$ the extension rate; the subscript c denotes the corresponding critical values.[13] For our precursor (surfactant/salt mixture), $\dot{\gamma}_c \approx 10\ s^{-1}$, $\dot{\varepsilon}_c \approx 10^6\ s^{-1}$, and $\gamma_c \approx 5000$. We used soft-lithography techniques to fabricate microdevices with size limitations on the order of 10 μm. To achieve the critical strains rates and strain for irreversible gelation, we inserted micrometer-sized glass particles into the flow: these particles jam the channel cross-section due to hydrodynamic forces and create an in-situ microporous medium. As the precursor passes through these narrow pores, the shear rates and extension rates shoot up by several orders of magnitude exceeding the strains required for nanoporous gel formation. Since the packing of the glass beads is not ideal (e.g., large gaps among the beads), the precursor is not sufficiently strained for gelation. As a result, the microporous flow produces a mixture of gels and liquid downstream of the microchannel. In short, we are able to use microfluidics to create a purely flow-induced, high extension-dominated flow (extension rate as high as $10^7\ s^{-1}$), allowing the surfactant solution to undergo permanent gelation and form stable, biocompatible nanoporous scaffolds under ambient conditions. Figure 1 shows the schematics of the microfluidics device for continuous production of nanoporous material. The generated gel sample was characterized by cryogenic transmission electron microscopy (cryo-TEM) with representative results shown in Figure 1A. The gel consists of highly aligned micelles with a short-range order. The alignment of the micelles results in the formation of nanochannels (grey arrows) and hole-like regions (black arrows). Image analysis yields the average nanochannel spacing, which is 41 ± 6 nm while the pore sizes are 27 ± 4 nm. The nanoporous scaffold formation enabled by microfluidics offers an ideal encapsulating environment for enzymes and other biomolecules. Although our method involves sol–gel transition or gelation, it is distinctly different from the conventional sol–gel method, which usually relies on either acid or base as a catalyst and uses alcoholic solvents.[14–17] Since the 1990's, there have been important advancements in the immobilization of enzymes and other biomolecules in the sol–gel matrices.[18–23] However, conventional sol–gel procedures generally result in entrapped biomolecules being partially denatured and aggregated.[18,19,22,23] Meanwhile for our new approach, the flow-induced nanoporous scaffold synthesis is facilitated and controlled by fluid mechanics with minimal or no usage of chemical and thermal means, and it is completely biocompatible.

In this work, we adopted the flow-induced gelation approach to encapsulate enzymes inside nanoporous scaffolds in a single step. We mixed the enzyme horseradish peroxidase (HRP) and

[*] Dr. D. L. Lu, J. Cardiel, Prof. A. Q. Shen
Department of Mechanical Engineering
University of Washington
Seattle, WA 98195 (USA)
E-mail: amyshen@uw.edu
Prof. G. Z. Cao
Department of Materials Science and Engineering
University of Washington
Seattle, WA 98195 (USA)

DOI: 10.1002/adma.201000189

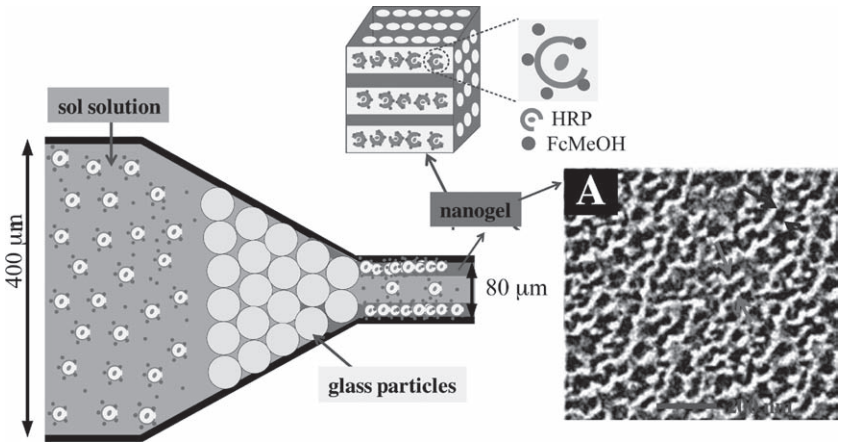

Figure 1. Schematic diagram of flow-induced gelation in a microfluic device. The inset (A) is a cryo-TEM image of nanogel formed in surfactant solutions by microporous flow. The sol solution contains CTAB (cetyl-trimethyl ammonium bromide) at a concentration of $C_1 = 0.05$ M, NaSal (where Sal is salicylate) at $C_2 = 0.015$ M, HRP at $C_3 = 1$ mg mL^{-1}, and FcMeOH at $C_4 = 5$ mM.

ferrocene methanol (FcMeOH) with the surfactant and salt as the precursor solution (or sol) before they are passed through the microfluidics setup (see Figure 1). The nanogel obtained after the sol passes through the glass particles provides a host matrix with enzymes and FcMeOH immobilized inside the porous scaffolds. This method allows enzymes to retain their functional characteristics to a large extent.

To verify the encapsulation of HRP and FcMeOH inside the gel, **Figure 2** shows the absorbance spectra of the nanogel. Absorption peaks of HRP at 406 nm and FcMeOH at 440 nm clearly indicate that both HRP and FcMeOH were encapsulated into the nanogel by the microfluidics setup.

The conventional covalent binding of an enzyme to a matrix generally requires specific functionalities to be present on the enzyme.[3,5] Here, the flow-induced gelation approach enables the entrapment of the enzyme HRP into nanoporous scaffolds and offers the following advantages. First, our encapsulation technique is independent of the functionalities on the HRP. Second, physical entrapment rendered in our approach is functionally noninvasive and preserves the integrity and directional homogeneity of the HRP surface microstructure. By contrast, covalent attachment of HRP via surface modification fixes the orientation of the exposed HRP and in certain cases may block substrate access to HRP's active site.[23] In addition, while the existing method of physical adsorption of an enzyme inside a nanotube or other porous material[6,7] is limited by the size of the pores and of the enzyme to be trapped, our flow-enhanced gelation method is largely independent of the size of the enzyme because the matrix forms around the enzyme during the gelation process. Moreover, we washed our nanogel with deionized (DI) water, and added 3,3′,5,5′-tetramethylbenzidine (TMB) liquid substrate to the collected DI water solution; no visible color change was observed after 30 min, indicating that the flow-induced nanoporous scaffolds can effectively prevent the leaching of enzyme molecules.

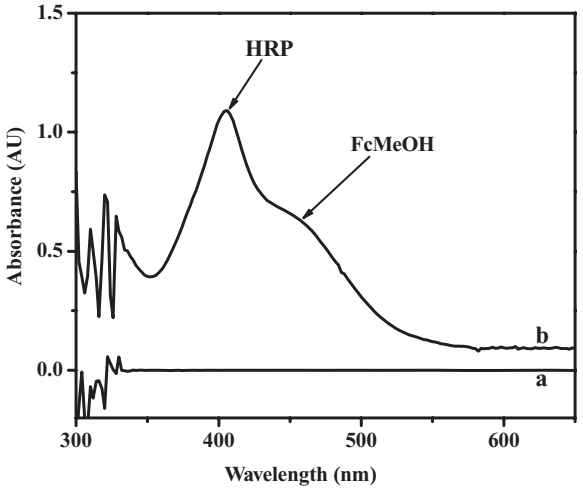

Figure 2. Absorbance of flow-induced nanogel (a) and with HRP and FcMeOH encapsulated (b). Experimental conditions are the same as those in Figure 1.

In addition, the nanogel with immobilized enzyme usually contains a sufficient amount of trapped interstitial water to provide a stable aqueous microenvironment, which is of utmost importance for maintaining the native stabilities and reactivities of HRP. As in an aqueous medium, the side chains of HRP interact with solvent water through hydrogen bonding and dipolar interactions. The recognition centers of the HRP are almost always exposed on the surface, and its sensitivity is usually maximized in an aqueous medium.[23]

After we obtain the nanogel with immobilized HRP and FeMeOH, we spin-coat the nanogel onto an indium tin oxide (ITO) electrode for electrochemical detection of hydrogen peroxide (H_2O_2). A basic ITO-based sensor is fabricated as follows. The substrate of ITO was firstly divided into three separate zones (working, counter, and pseudoreference electrode) with 30 min of hydrochloric acid (6 M) etching. Nanogel (1 μL) was cast onto the center of the ITO substrate, and formed a thin layer to cover the top of the three electrodes after spin-coating. The cyclic voltammetric response of the hydrogen peroxide biosensor is shown in **Figure 3**. In a blank nanogel with no hydrogen peroxide, the biosensor only exhibited the electrochemical behavior of FcMeOH, a pair of anodic and cathodic waves (curve a). With the addition of H_2O_2, the cathodic peak current increased and the anodic peak current decreased significantly (curve b). This indicates that the nanogel-coated biosensor can be utilized for the detection of trace levels of H_2O_2.

We also compared the amperometric response of the nanogel-based H_2O_2 sensor and a H_2O_2 sensor fabricated using Nafion for a sensitivity study. For comparison purposes, we used the same initial HRP concentration in the Nafion solution and the precursor solution for the nanogel production. The Nafion-based sensor uses entrapment, a conventional method for enzyme immobilization. The Nafion sensor fabrication is

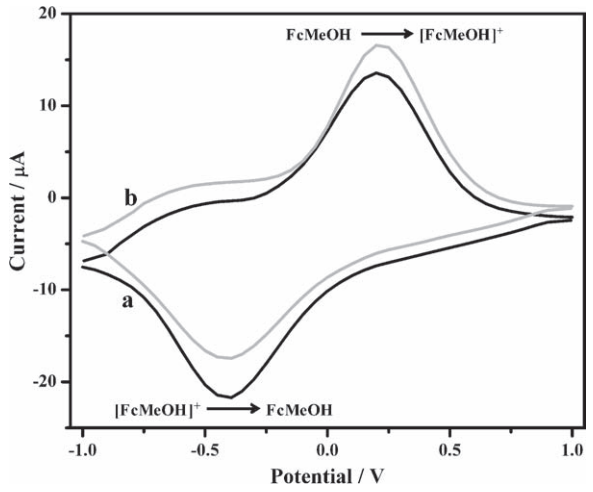

Figure 3. Cyclic voltammograms of nanogel-coated biosensor in the absence (a) and presence (b) of 0.1 mM H_2O_2 at a scan rate of 100 mV s^{-1}. Conditions are the same as those specified in Figure 1.

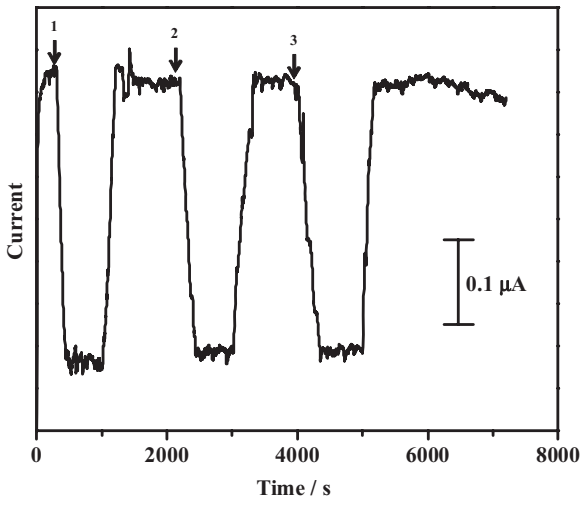

Figure 5. Amperometric response of nanogel-based biosensor for three successive measurements of 0.1 mM H_2O_2 over a 2 h operation period.

described in detail elsewhere.[24] In summary, 1 μL of 10 mM phosphate buffer solution containing 1 mg mL^{-1} HRP and 5 mM FcMeOH were cast onto the ITO electrode surface. The electrode was dried at room temperature (~25 °C) for 30 min. Finally, about 3 μL of 1% Nafion (in 95% alcohol) was deposited onto the electrode surface and dried. The electrode was stored in the refrigerator when not in use. For both sensors, successive injections of 0.1 mM H_2O_2 at an applied potential of –0.5V is applied, as shown in **Figure 4A**. For the Nafion-based H_2O_2 sensor, an insignificant current response was observed after the addition of H_2O_2 (curve c). In contrast, a larger and well-defined current (close to 4 times higher) was obtained with the nanogel-modified ITO electrodes (curve d) with similar HRP content inside the nanoporous matrix. The performance displayed in Figure 4A confirms that the nanogel-based sensor exhibits higher sensitivity compared to the Nafion-based sensor, with the same HRP content (1 mg mL^{-1}). The possible reason for the higher sensitivity displayed by the nanogel sensor could be that the nanoporous scaffold provides a desirable nanoporous matrix to prevent HRP leakage, and forms a more stable aqueous microenvironment to maintain the HRP activity. Ongoing research to evaluate and quantify the enzyme bioactivity inside the nanogel for more effective enzyme and other bimolecular encapsulation will be reported in the future.

The calibration plot of the hydrogen peroxide biosensor is shown in Figure 4B. As expected, the response of the nanogel-based biosensor to H_2O_2 was linear in the range of 0.1–1.5 mM with a detection limit of 2.5 μM (signal-to-noise ratio, $S/N = 3$), while the Nafion-based sensor only has a detection limit of 20 μM.

A relative standard deviation (RSD) of 2.4% is observed over a 2 h operation period (see **Figure 5**) of amperometric response from the nanogel-based biosensor for three successive measurements. We also investigated the stability and selectivity of the nanogel-based biosensor. The stability of the biosensor was studied by amperometric measurements in the presence of

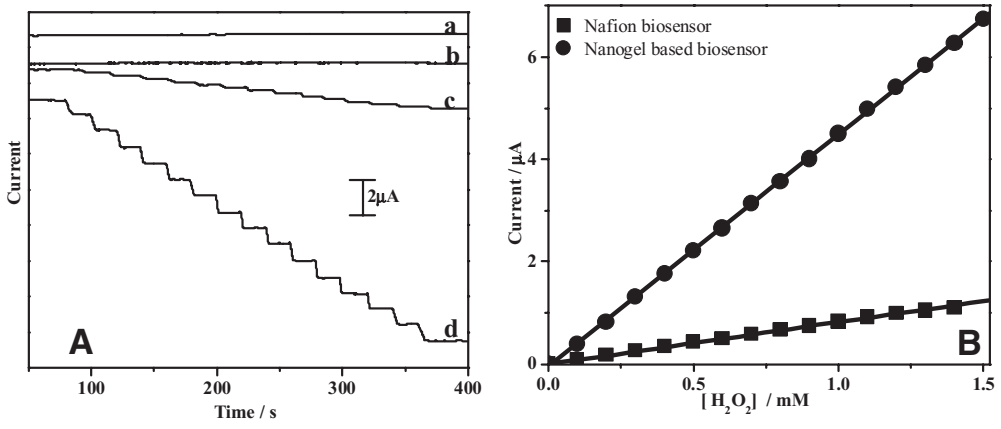

Figure 4. A) Amperometric response of Nafion- (c) and nanogel- (d) based biosensor upon successive additions of 0.1 mM H_2O_2 along with the background for Nafion (a) and nanogel (b), respectively. B) The calibration curve of the biosensor. Experimental conditions are the same as those of Figure 1.

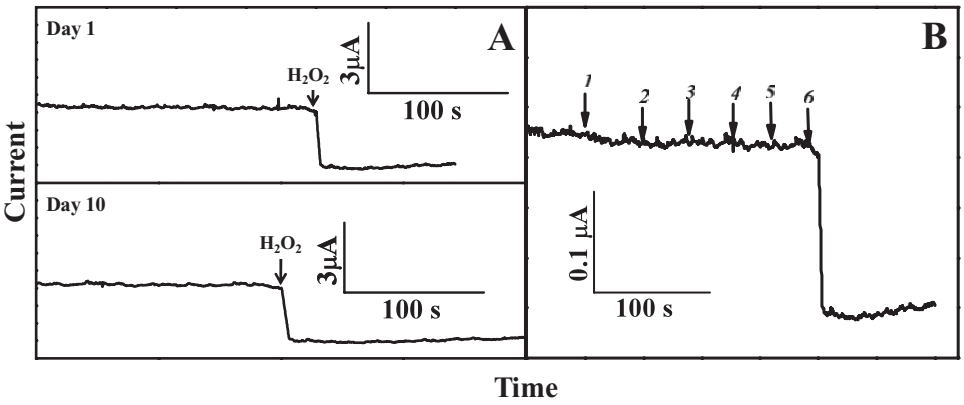

Figure 6. Amperometric response of nanogel-based biosensor upon the detection of A) 1 mM H_2O_2 at day 1 and day 10, respectively, and B) 0.1 mM H_2O_2 (6) in the presence of the 0.2 mM ascorbic acid (1), acetic acid (2), ethanol (3), L-leucine (4), and L-tyrosine (5).

1 mM H_2O_2 periodically (see **Figure 6A**). When not in use, the nanogel-based sensor was stored under high humidity (relative humidity, RH > 90%) at 25 °C. The biosensor lost only 3.5% of the initial response after 10 days. Both the precision and stability studies verify that the enzyme's activity is preserved over a long period of time.

We also demonstrated highly selective detection of H_2O_2 with various common interferents such as ascorbic acid, acetic acid, ethanol, L-leucine, and L-tyrosine (see Figure 6B). In our experiments, the five tested substances did not interfere significantly with the nanogel-based biosensor for trace levels of H_2O_2 detection.

In conclusion, a truly simple, fast, and cost-effective flow-induced gelation procedure to immobilize enzymes is introduced. Our new approach used microfluidic devices to facilitate the single-throughput, in-situ process to immobilize enzymes in a nanoporous scaffold that can retain the enzymes' native stabilities and reactivities. The nanoporous gel provides the favorable host matrix that isolates the enzyme molecules, protecting them from self-aggregation and leaching, while providing essentially the same local aqueous microenvironment as in biological media. The nanogel-based biosensor has demonstrated a highly linear amperometric response over the 0.1–1.5 mM range, in which H_2O_2 presence was examined at a high sensitivity of 2.5 μM, a high stability and selectivity, and good precision (RSD = 2.4%). This flow-induced immobilziation technique opens up new pathways for designing simple, fast, biocompatible, and cost-effective processes for enhanced sensor performance and on-site testing of a variety of biomolecules.

Experimental Section

Apparatus and Reagents: The microfluidic devices were fabricated by soft-lithography techniques, with polydispersed (30–50 μm) glass particles (Polysciences, Inc.) accumulating near the constriction and forming a pseudopacked bed (Figure 1). We can obtain a high shear rate and strain within the microporous flow region, which are above critical shear rate ($\dot{\gamma}_c \approx 10\ s^{-1}$) and critical strain ($\gamma_c \approx 5000$) for shear-induced structural formation (Supporting Information, SI).

Electrochemical measurements (cyclic voltammetry and amperometry) were conducted using an electrochemical analyzer CHI 1232A (CH Instruments, Austin, TX) connected to a personal computer. A basic version of the biosensor is constituted of merely a substrate of ITO-printed electrodes (working, counter, and pseudoreference electrode) and a thin layer of nanogel covering on top.

CTAB (99.5%) was purchased from Fluka. NaSal (99.5%), HRP (2.5 mg mL^{-1}), FcMeOH (97%), TMB liquid substrate, and hydrogen peroxide (30% w/v solution) were purchased from Sigma. Chemicals were of reagent grade and were used as received. All solutions were prepared with DI water (>16 MΩ cm^{-1}).

Acknowledgements

The project was supported by grants from National Science Foundation, NSF-CAREER 0645062 (AQS).

Supporting Information

Supporting Information is available online from Wiley InterScience or from the authors.

Received: January 16, 2010
Revised: March 9, 2010
Published online: April 29, 2010

[1] J. Wang, D. K. Xu, A. N. Kawde, R. Polsky, *Anal. Chem.* **2001**, *73*, 5576.
[2] I. Willner, A. Riklin, B. Shoham, D. Rivenzon, E. Katz, *Adv. Mater.* **1993**, *5*, 912.
[3] F. Fernández Trillo, J. C. M. van Hest, J. C. Thies, T. Michon, R. Weberskirch, N. R. Cameron, *Adv. Mater.* **2009**, *21*, 55.
[4] G. D. Liu, Y. H. Lin, *Anal. Chem.* **2006**, *78*, 835.
[5] M. Hartmann, *Chem. Mater.* **2005**, *17*, 4577.
[6] J. Lee, J. Kim, T. Hyeon, *Adv. Mater.* **2006**, *18*, 2073.
[7] P. Xiao, B. B. Garcia, Q. Guo, D. W. Liu, G. Z. Cao, *Electrochem. Commun.* **2007**, *9*, 441.
[8] J. Wang, *Electroanalysis* **2005**, *17*, 7.
[9] S. E. Letant, B. R. Hart, S. R. Kane, M. Z. Hadi, S. J. Shields, J. G. Reynolds, *Adv. Mater.* **2004**, *16*, 689.
[10] D. Lee, J. Lee, J. Kim, H. B. Na, B. Kim, C. H. Shin, J. H. Kwak, A. Dohnalkova, J. W. Grate, T. Hyeon, H. S. Kim, *Adv. Mater.* **2005**, *23*, 2828.
[11] M. Gerard, A. Chaubey, B. D. Malhotra, *Biosens. Bioelectron.* **2002**, *17*, 345.

[12] I. Gill, A. Ballesteros, *J. Am. Chem. Soc.* **1998**, *120*, 8587.
[13] M. Vasudevan, E. Buse, D. L. Lu, A. Q. Shen, B. Khomami, R. Sureshkumar, *Nat. Mater.* **2010**, DOI: 10.1038/nmat2724.
[14] C. Liu, D. J. Pine, *Phys. Rev. Lett.* **1996**, *77*, 2121.
[15] N. K. Raman, M. T. Anderson, C. J. Brinker, *Chem. Mater.* **1996**, *8*, 1682.
[16] B. B. Lakshmi, C. J. Patrissi, C. R. Martin, *Chem. Mater.* **1997**, *9*, 2544.
[17] Y. F. Lu, R. Ganguli, C. A. Drewien, M. T. Anderson, C. J. Brinker, W. L. Gong, Y. X. Guo, H. Soyez, B. Dunn, M. H. Huang, J. I. Zink, *Nature* **1997**, *389*, 364.
[18] M. T. Reetz, A. Zonta, J. Simpelkamp, *Biotechnol. Bioeng.* **1996**, *49*, 527.
[19] G. Z. Cao, Y. F. Lu, L. Delattre, C. J. Brinker, G. P. Lopez, *Adv. Mater.* **1996**, *8*, 588.
[20] H. Y. Fan, A. Wright, J. Gabaldon, A. Rodriguez, C. J. Brinker, Y. B. Jiang, *Adv. Funct. Mater.* **2006**, *16*, 891.
[21] R. B. Bhatia, C. J. Brinker, A. K. Gupta, A. K. Singh, *Chem. Mater.* **2000**, *12*, 2434.
[22] U. Narang, P. N. Prasad, F. V. Bright, K. Ramanathan, N. D. Kumar, B. D. Malhotra, M. N. Kamalasanan, S. Chandra, *Anal. Chem.* **1994**, *66*, 3139.
[23] B. C. Dave, B. Dunn, J. S. Valentine, J. I. Zink, *Anal. Chem.* **1994**, *66*, 1120.
[24] T. Feng, Y. Yang, M. Chuang, S. Luo, M. Galik, G. Flechsig, J. Wang, *Electrochem. Commun.* **2009**, *11*, 1812.